JOURNAL OF MATERIALS SCIENCE 23 (1988) 515–522

Crystallization processes in an Ni–Si–B glassy alloy

M.-H. ZUERCHER, D. G. MORRIS
Institute of Structural Metallurgy, University of Neuchâtel, 2000 Neuchâtel, Switzerland

The crystallization of metallic glasses is often conveniently separated into distinct nucleation and growth processes. The nucleation or formation of crystals is a poorly understood stage which may depend on many properties of the alloy in question as well as on the preparation conditions. Nucleation may involve internal homogeneous or heterogeneous mechanisms or localized, surface processes. An easy glass-forming alloy has been examined after preparation under clean, and very-fast-cooling conditions. These careful preparation conditions have significantly slowed crystallization kinetics by slowing the bulk nucleation kinetics. Accordingly the material shows an extreme sensitivity to surface contamination and intensive associated crystal nucleation: in addition the inner parts of the material crystallize by an apparently homogeneous nucleation process. The results obtained are important in emphasizing the role of quenched-in structures and contaminants on enhancing crystal nucleation activity. An improved understanding of these factors could play a significant role in the development of more-stable, or larger-bulk metallic glasses.

1. Introduction

The study of the crystallization of metallic glasses is of fundamental interest as this represents a phase transformation occurring under extreme conditions far from equilibrium. The subject is also of real technological interest because of the inter-relation of crystal formation from the glass to its preparation and stability, as well as because of the possibility of using glasses as a starting point for producing desirable fine microstructures of stable or metastable phases by controlled crystallization.

Of particular interest is the study of crystal nucleation processes during such transformations. Several categories of nucleation process have been identified [1], ranging from homogeneous nucleation through heterogeneous mechanisms to the simple growth of pre-existing, quenched-in crystals: in addition, localized, heterogeneous nucleation at free surfaces has sometimes been observed. At high temperatures, the classical homogeneous nucleation mechanism may be expected to dominate crystallization, whilst at low temperature there may be a considerable incubation period, required to build up the stable embryo distribution, before steady-state nucleation is achieved [1, 2].

The classical homogeneous nucleation model has been extensively used as a basis for modelling glass formability – based on the difficulty of forming crystals (e.g. [3, 4]). Such models are based on the belief that crystal nucleation during cooling will be essentially dominated by homogeneous nucleation, and several earlier studies have confirmed the importance of this nucleation mode [5, 6].

More recently the importance of inhomogeneous nucleation has been increasingly noted, either as a limited extent of bulk nucleation [7, 8] or as kinetics of crystal appearance which are clearly incompatible with homogeneous nucleation [9, 10]. The inhomogeneous, volume nucleation mechanisms can essentially be separated into two types – those dependent on quenched-in structures, and those dependent on impurity atoms or particles. An example of the inhomogeneous nucleation mechanism is given by Greer [11], who showed differing crystal nucleation kinetics when annealing Fe–B glasses prepared at different quenching rates – in this case it may be considered that the intrinsic, quenched-in structure of the glass, or eventually the presence of quenched-in clusters, controls nucleation. The importance of impurity effects is well illustrated by the current attempts to improve glass formability, or to obtain "massive" glassy samples by purifying and avoiding surface contamination of a cooling melt [9].

The present work considers the crystallization processes within an Ni–Si–B glass. This alloy system contains easy glass-forming compositions [12] and several glasses in this system have previously been examined from a viewpoint of the crystallization temperatures [12–15] or of the crystallization kinetics [16, 17]. The present study considers the crystallization response of such a glassy alloy prepared under conditions where both the quenched-in, intrinsic clustering, as well as impurity effects, are minimized – namely by casting the ribbon under clean and inert conditions using a very high quenching speed. In particular a comparison of the crystallization mode and kinetics with previous data will allow a detailed evaluation of such inhomogeneous nucleation phenomena.

In view of the wide variety of crystallization modes which is possible, it has been preferred to choose the

0022–2461/88 $03.00 + .12

most direct techniques for evaluation of the transformation, namely using quantitative metallographic techniques. The use of such techniques has, at the same time, allowed the examination of unexpected surface crystallization mechanisms, and the interpretation of these bears directly on the analysis of the volume nucleation process.

2. Experimental procedure

The alloy used has a composition of nickel–7% silicon–17% boron (atomic per cent) and was prepared by induction melting quantities of the pure elements under vacuum in a quartz tube: the precise composition was confirmed using absorption spectroscopy. The alloy was cast as ribbon about 3 mm wide and 30 μm thick using melt spinning: the quenching substrate was a polished copper wheel moving at 26 m sec^{-1} and the casting environment was 0.5 bar helium obtained after first evacuating and flushing the container vessel with helium. The precise conditions used for casting were determined following the guidelines given by Pavuna [18].

Samples were isothermally treated at temperatures between 400 and 470° C: lower temperature anneals were performed under argon protection whilst the highest temperature, short-time anneals were carried out using a salt bath – control experiments confirmed that the same crystallization response was obtained, independent of the annealing environment.

Sample analysis was carried out mainly by optical microscopy, also using scanning electron microscopy when higher resolution was required. Photographs obtained were analysed using a Quantimet 520 image analyser. Crystal size distributions were determined in some cases, using either optical or electron micrographs as necessary. Large numbers of crystals (500 to 1000) were counted on each sample to improve the accuracy of the statistical analysis. Distributions were deduced using both the Schwartz–Saltikov and the Dehoff analyses [19, 20]: the former analysis gave more satisfactory results.

Crystal phase analysis was performed by transmission electron microscopy on thin foils, prepared using a solution of 10% perchloric acid in ethanol at about – 10° C and 20 V.

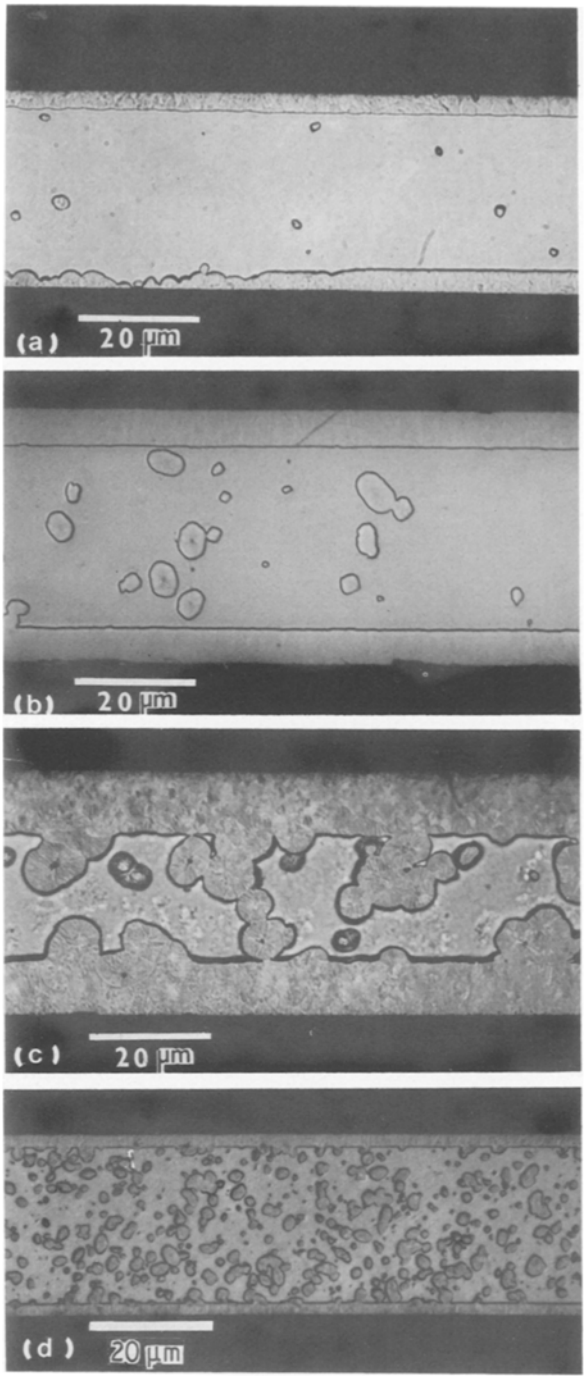

Figure 1 Micrographs illustrating the simultaneous surface and internal crystallization of the Ni–7Si–17B alloy: (a) 25 h at 400° C, (b) 50 h at 400° C, (c) 60 h at 400° C, (d) 45 min at 450° C.

3. Results

Cross-sections through typical, partially-crystallized materials are illustrated in Fig. 1. All samples exhibit simultaneous surface and bulk crystallization. The surface nucleation is highly prolific and the growth of the surface, crystalline layer takes place at about the same rate as for the internal crystals. At higher temperature there is more extensive internal nucleation, as seen by comparing Figs 1a to c and Fig. 1d.

3.1. Surface crystallization

An important observation made on each sample is the very high rate of surface crystallization. Already for very short annealing times, where bulk crystallization can hardly be detected, a surface crystallized region is distinctly visible – initially in the form of semi-circular crystal sections already touching each other, and very soon afterwards in the form of a virtually straight interface between the crystalline surface and the glassy interior.

For each annealing temperature and time, the width of the crystallized edge of the ribbon is approximately half the diameter of the largest crystals within the bulk, see Fig. 2. The growth rate at a crystalline interface can thus be taken as constant for a given temperature, and can be assumed to occur by the same mechanism for a near-surface interface and an internal-crystal interface.

Many different tests have been performed to determine the origin of the rapid crystallization at the surface. Firstly, the heat treatments have been carried out under several different conditions of environment (in flowing argon, in open atmosphere, sealed in

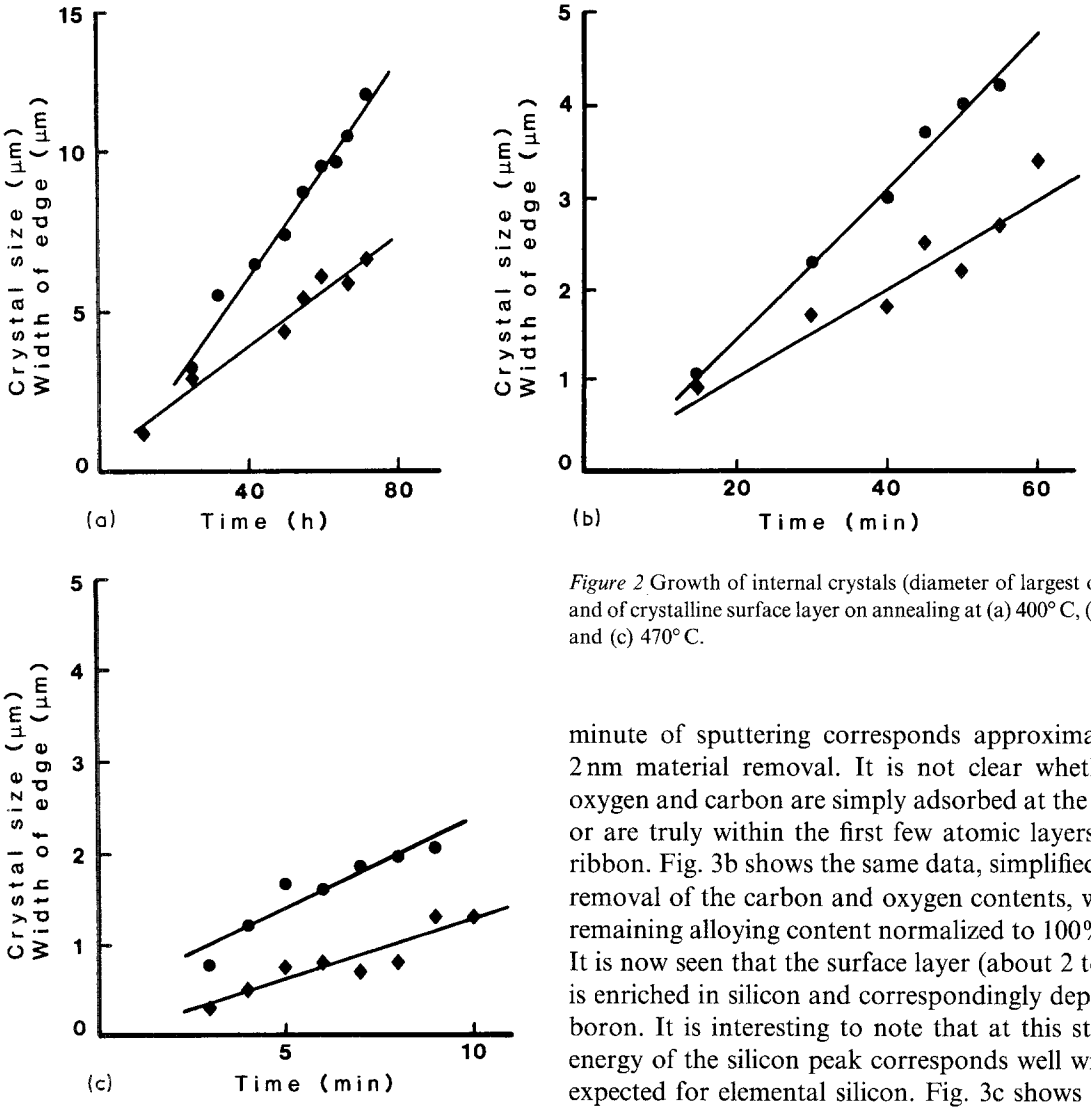

Figure 2 Growth of internal crystals (diameter of largest observed) and of crystalline surface layer on annealing at (a) 400° C, (b) 450° C and (c) 470° C.

quartz tube under a vacuum of 10^{-3} Pa). No difference in the appearance or width of the crystallized layers has been observed. Secondly, annealing has been carried out (under argon) after abrading or after polishing the ribbon surfaces to eliminate the possible effects of local contamination during the melt-spinning process itself. In this case again, the same extensive surface crystallization was observed, and it can be concluded that effects specific to the melt-spinning process are not responsible for the enhanced nucleation. (This conclusion is, in fact, already evident from the similarity of nucleation at the two surfaces, wheel and free side, of the ribbon.) Finally, to examine the influence of possible mechanical effects such as superficial stress or strain occurring during ribbon fabrication or handling, we have compared the crystallization response of as-cast, of electroplated and of elastically and plastically bent ribbons: again identical crystallization kinetics were observed with no influence of these parameters.

To provide more information on the surface state, Auger electron spectroscopy (AES) has been used. Detailed Auger spectra have been obtained after varying degrees of sputter-etching, as well as depth-profiles of the major elements detected, see Fig. 3. Fig. 3a shows the profiles of the three alloying elements, as well as oxygen and carbon, observed on the as-cast material as a function of the sputtering time. Each minute of sputtering corresponds approximately to 2 nm material removal. It is not clear whether the oxygen and carbon are simply adsorbed at the surface or are truly within the first few atomic layers of the ribbon. Fig. 3b shows the same data, simplified by the removal of the carbon and oxygen contents, with the remaining alloying content normalized to 100% total. It is now seen that the surface layer (about 2 to 3 nm) is enriched in silicon and correspondingly depleted in boron. It is interesting to note that at this stage the energy of the silicon peak corresponds well with that expected for elemental silicon. Fig. 3c shows profiles of the three alloying elements observed after annealing (under a vacuum of 10^{-3} Pa) to the beginning of surface crystallization. Carbon and oxygen, detected to a depth of 4 to 5 nm, have been removed from this figure to simplify interpretation. In Fig. 3c it is clearly seen that the surface layers (about 4 to 5 nm) have become enriched in silicon, with a corresponding depletion of nickel as well as, slightly, of boron. The energy of the silicon peak at the surface corresponds now to that of silica-oxidized silicon.

3.2. Bulk crystallization

In this section the nucleation and growth rates of the crystals observed within the glass volume are described, as well as the analysis of the crystallographic structure.

The growth rates of the internal crystals have already been shown in Fig. 2. It should be noted that the growth rate observed remains constant at each temperature, with an increasing growth rate at higher temperature. This increase is well described by an Arrhenius relationship with an activation energy of 250 kJ mol^{-1}.

The variation of crystal number density with annealing temperature and time is shown in Fig. 4. The volume density of crystals, N_v, has been deduced using

$$N_v = N_a/\phi$$

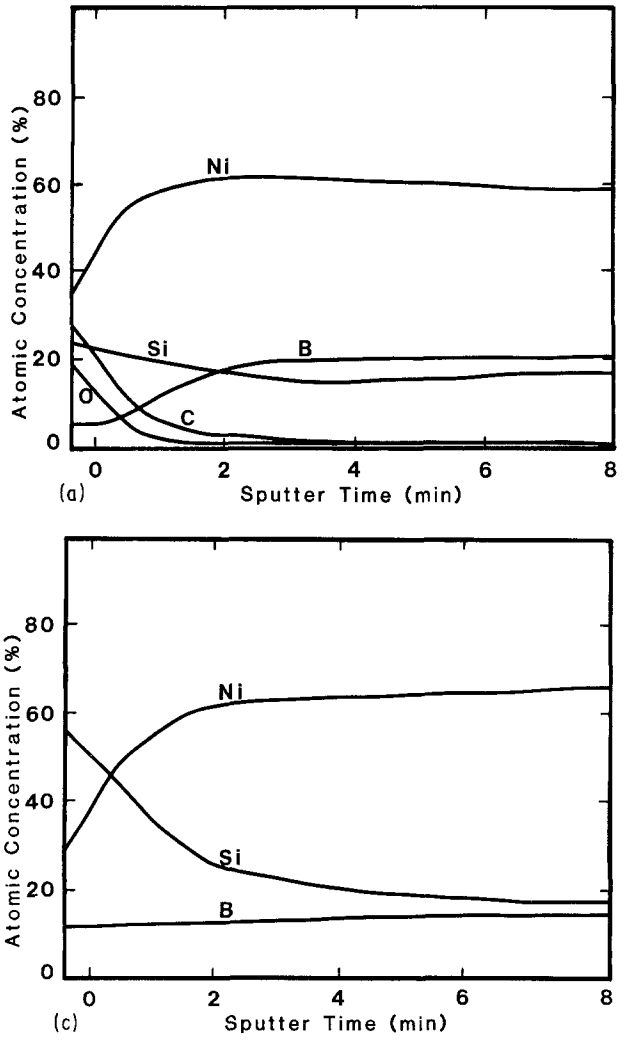

Figure 3 Auger electron spectroscopy composition profiles observed during sputter-etching (each minute removes about 2 nm of surface): (a) and (b) profiles obtained on as-cast ribbon, in (b) the carbon and oxygen profiles have been removed and the remaining element contents normalized to 100%; (c) the profiles obtained after annealing for 45 min at 450° C, to the beginning of crystallization – again the carbon and oxygen profiles have been removed.

where N_a is the surface crystal density and ϕ the average diameter of the crystals. The data at 400° C show a different behaviour relative to the other temperatures, namely a sharp increase in crystal density from the beginning of crystallization, reaching an approximately constant value at an early stage, when less than 10% of the sample volume has crystallized. This behaviour, namely a rapid, early nucleation to a saturation value, about 2×10^{15} crystals per m^3, is typical of a nucleation process occurring on a pre-existing, quenched-in embryo distribution within the glass; once these embryos are used nucleation essentially stops. In fact it appears that nucleation probably continues at a very low rate, about 10^9 crystals per m^3 per sec.

At 450 and 470° C, however, nucleation occurs at a steady rate over the entire range of crystallization studied, indicating a continuous, uniform nucleation process. It should be noted that the straight lines obtained do not extrapolate exactly through the origin – a short transient nucleation stage is evident at 450° C whilst at 470° C the data extrapolate to a positive, small crystal density at zero time. The steady state nucleation data (including the approximate value corresponding to 400° C) are shown, in Fig. 5, to obey an Arrhenius relationship with an activation energy of 690 kg mol^{-1}.

Information obtained on the crystal-size distribution is essentially consistent with the nucleation and growth modes observed, and will be discussed later.

Transmission electron microscopy was used to examine the internal crystal morphology at higher magnification and also to identify the phase structure by diffraction analysis, Fig. 6. The crystals are identified as single-phase crystals of the orthorhombic Ni_3B-type phase. It appears that the silicon atoms are able to substitute for boron in this phase, and that the slight difference of alloy composition from stoichiometry (the alloy has 76% nickel) does not lead to element rejection or second-phase formation. These results are in agreement with previous analyses [16, 17].

4. Discussion

4.1. Surface crystallization

The experiments described earlier concerning the influence of many different surface states and annealing environments on surface crystallization make it possible to deduce fairly precisely the origin of the phenomenon. The effects of gross contamination at the surfaces, whether occurring during melt-spinning or during annealing, as well as the effects due to mechanical strains, could all be essentially removed without affecting the surface behaviour. These observations are substantially different from earlier studies where, for example, a pronounced effect of the spinning wheel contact surface is observed [21] resulting in preferential crystallization on one side of the ribbon. In other cases, selective oxidation [1] or surface mechanical treatments [22] such as induced by cold rolling and sharp bending have clearly enhanced surface crystallization.

From another point of view, it appears clearly that the reduction of nucleation barrier at a surface or corner, as described by Christian [2], is not sufficient to explain the very enhanced nucleation detected at the surfaces. If such a reduction were significant,

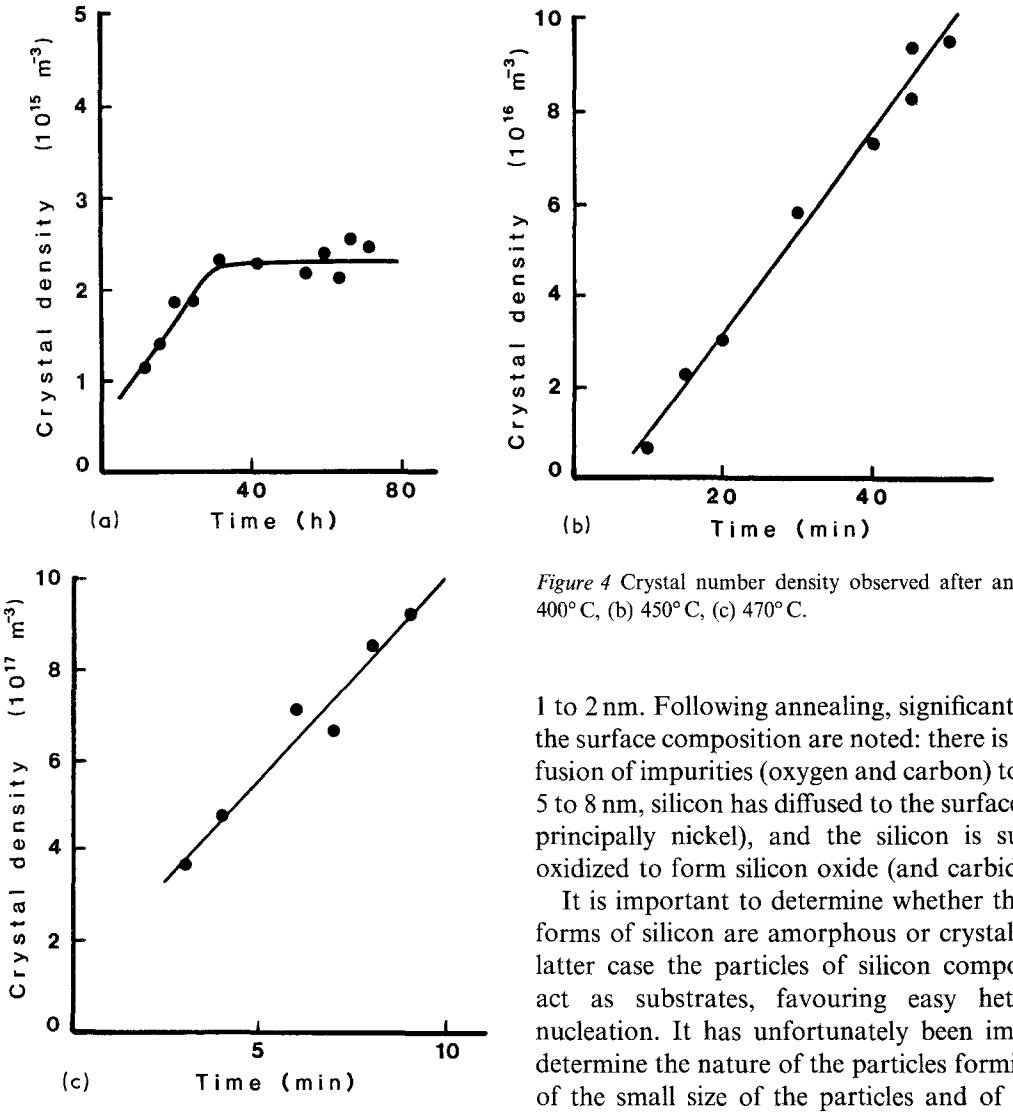

Figure 4 Crystal number density observed after annealing at (a) 400° C, (b) 450° C, (c) 470° C.

surface nucleation would be virtually a standard nucleation mode for all metallic glasses.

Finally, the Auger electron spectroscopic results have allowed us to make a precise analysis of the surface behaviour. AES data on the as-cast ribbon surface detect carbon and oxygen impurities, probably adsorbed. The data obtained following sputter-etching confirm that the contamination is limited to the first 1 to 2 nm. Following annealing, significant changes in the surface composition are noted: there is inward diffusion of impurities (oxygen and carbon) to a depth of 5 to 8 nm, silicon has diffused to the surface (replacing principally nickel), and the silicon is substantially oxidized to form silicon oxide (and carbide).

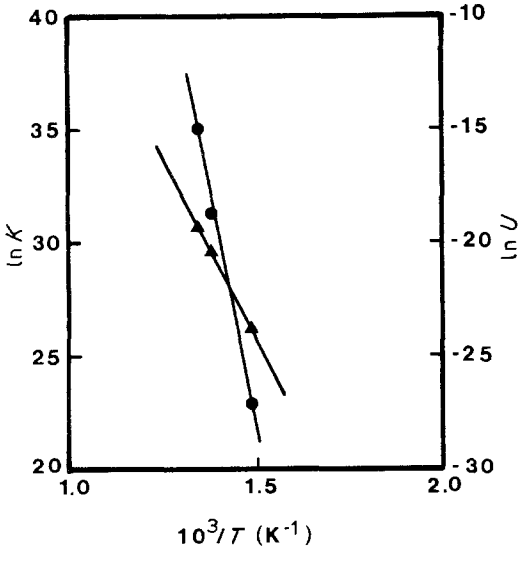

Figure 5 Arrhenius plots showing the variation of (●) nucleation and (▲) growth rates with temperature.

It is important to determine whether these reacted forms of silicon are amorphous or crystalline. In the latter case the particles of silicon compound could act as substrates, favouring easy heterogeneous nucleation. It has unfortunately been impossible to determine the nature of the particles forming, in view of the small size of the particles and of the surface layer within which they may form (probably less than 1 to 2 nm). According to earlier studies of the structure of silica formed by precipitation within crystalline silicon [23] it would seem likely that the particles formed within the metallic glass are amorphous. The AES data confirm that the remaining metallic glass of the surface region has significantly different chemical composition from that of the stable glassy volume. It is this effect which has most probably reduced the local crystallization temperature to such an extent that nucleation takes place readily. Following such abundant nucleation, the crystals formed grow through the surface-modified layer into the glass volume by precisely the same process as for growth of the internal crystals.

4.2. Bulk crystallization at low temperature

For the lowest annealing temperature, 400° C, we observed a crystallization behaviour similar to that previously seen on alloys of similar composition [16], namely an increase in crystal density at the beginning of crystallization and then a saturation when only about 5 to 10% of the alloy has transformed. The crystal density may subsequently increase at a very slow, steady rate, but the total number remains very low at about 2×10^{15} m^{-3}.

This behaviour suggests that a kind of continuous nucleation occurs initially. Growth occurs after the nucleation on quenched-in embryos, uniformly frozen

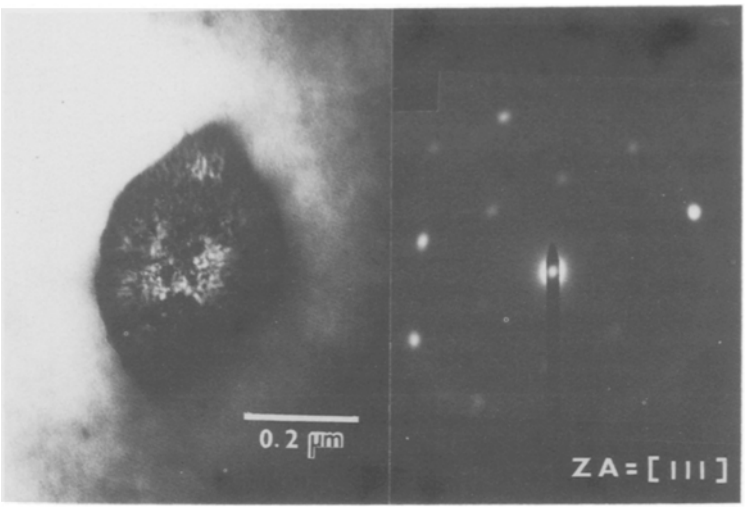

Figure 6 Electron micrograph and associated diffraction pattern [1 1 1] zone axis illustrating the typical crystal morphology, and identifying the crystal as a monophase orthorhombic Ni_3B structure.

in the alloy during the quenching process. This nucleation rate diminishes to zero as the quenched-in population is exhausted. The crystal-size distribution observed on partially crystallized samples reveals clearly that growth did not start at one single instant, but that crystal nucleation took place over a noticeable time period.

The steady-state nucleation rate observed after the initial nucleation period is very low, of the order of 10^9 crystals per m^3 per sec. This extremely low value is a reflection of the inherent stability (or resistance to crystallization) of the glass.

We thus deduce a two-stage nucleation characteristic for this alloy: initial rapid nucleation on a relatively low number of quenched-in inhomogeneities, subsequent slow and steady-state uniform nucleation. It is interesting to speculate on the possible origin of the quenched-in embryos – are they quenched-in intrinsic clusters (short-range ordered arrangements of the alloying elements) or quenched-in extrinsic clusters (associated with contaminants, such as internal oxygen)? In view of the lack of direct oxidation effect on surface nucleation (enhanced surface nucleation was obtained because of local alloy composition change as a result of silicon depletion) it would seem that quenched-in intrinsic clusters are probably responsible for the internal, rapid, initial nucleation. Further experiments using varying quenching rate and varying contaminant content are planned to test these deductions.

4.3. Homogeneous bulk crystallization

The nucleation behaviour observed at the higher temperatures (450 and 470° C) seems easier to understand. Linear nucleation and growth are observed at both temperatures, see Figs 2 and 4, over the entire range of crystallization. Analogous nucleation and growth also appears at 400° C after the initial fast nucleation period. It therefore follows that homogeneous nucleation probably occurs as a thermally activated process on a steady-state embryo distribution. There is only slight evidence for an incubation

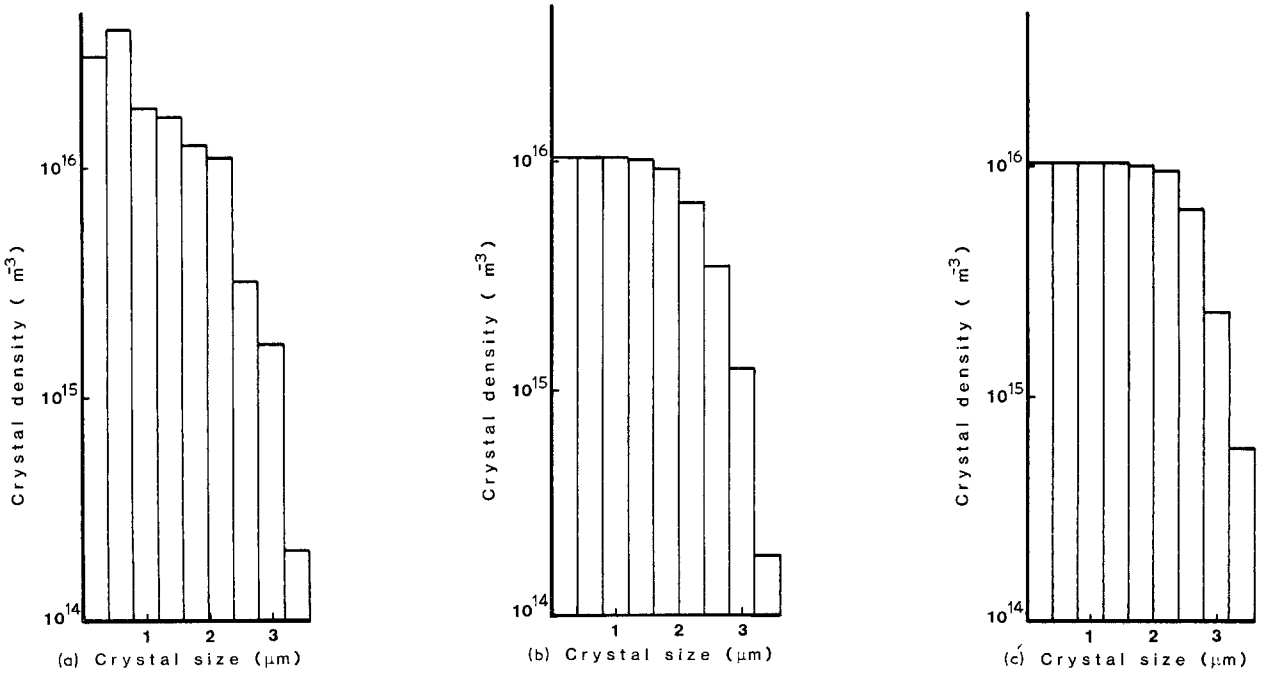

Figure 7 Crystal-size distributions corresponding to annealing for 45 min at 450° C showing the influence of transient nucleation; (a) measured distribution using the Schwartz–Saltykov analysis; (b) calculated distribution assuming a transient time, τ, of 8 min; (c) calculated distribution assuming a transient time, τ, of 6 min.

period to establish the steady state distribution, see later.

This change in nucleation behaviour with temperature, namely a continuous, steady-state nucleation at higher temperatures and a rapid near-saturation in nucleation at lower temperatures is essentially a consequence of the strong temperature dependence of the steady-state nucleation process. Thus at low temperatures the difficulty – or slowness – of steady-state nucleation means that quenched-in inhomogeneities dominate. Similar observations have previously been made on Fe–Ni–B glasses [21, 24]. The temperature dependences of nucleation and growth are interpreted in terms of thermally activated processes with activation energies of 690 and 250 kJ mol^{-1}, respectively, see Fig. 5.

Assuming that the deduced activation energy for growth is the same as that for atomic diffusion, Q_{diff} [25, 26], the activation energy corresponding to nucleation can be analysed using

$$I = I_0 \exp\left(\frac{-Q_{diff}}{kT}\right) \exp\left(\frac{-\Delta G^*}{kT}\right)$$

where I is the observed nucleation rate at the temperature T, I_0 is a constant and k the Boltzmann constant. Thus the deduced activation energy for nucleation, Q_n, can be written

$$Q_n = Q_{diff} + \Delta G^*$$

ΔG^* is the energy required to form the critically sized embryo, and is related to the crystal–glass interface energy, γ, and the volume free energy difference between glass and crystal, ΔG_v, as

$$\Delta G^* = 16\gamma^3/3(\Delta G_v)^2$$

Taking the value of γ as about 0.1 J m^{-3}, and the expression proposed by Thompson and Spaepen [27] for ΔG_v,

$$\Delta G_v = \frac{2\Delta H_v^f \Delta T_r T_r}{(T_r + 1)}$$

where ΔH_v is given [3] by $1.2RT_m\varrho/M$ (where M is the molar mass, ϱ the density, T_m the melting point and R the gas constant, T_r is T/T_m and ΔT_r is $(T_m - T)/T_m$) we obtain $\Delta G^* = 355$ kJ mol^{-1}. This value is in good agreement with the value deduced from the experimental data, $\Delta G^* = Q_n - Q_{diff} = 690$ to $250 = 410$ kJ mol^{-1}. Note that an increase in the presumed value of γ from 0.1 to 0.11 J m^{-2} is sufficient to increase the calculated value of ΔG^* to larger than the experimentally deduced value. Accordingly, we conclude that the experimental data are totally consistent with a homogeneous nucleation process.

Another feature of nucleation to be noted in Fig. 4, particularly the data at 450° C, is the clear evidence of an incubation period, τ, during which the steady-state embryo distribution is being built up and classic nucleation is not yet occurring at the equilibrium rate. This transient nucleation has received considerable attention from a theoretical point of view [28, 29] as well as experimentally [21, 30]. Taking such transient effects into account, the almost uniform size distribution obtained during steady-state homogeneous nucleation will be strongly modified [24, 31].

Such distributions were established in our study for several different heat treatments using both the Schwartz–Saltykov and Dehoff methods [19, 20]. Both methods gave similar general distributions but with noticeably different numbers of particles within each class: because the Schwartz–Saltykov analysis gave more correct values, this method was selected for further study of size distributions.

Fig. 7a illustrates the distribution obtained using this method on a sample annealed for 45 min at 450° C. According to Kashchiev [32] the transient or time-dependent nucleation rate, $I(t)$, is given by

$$I(t) = I_{ss}\left[1 + 2\sum_{n=1}^{\infty}(-1)^n \exp\left(-\frac{n^2 t}{\tau}\right)\right]$$

where I_{ss} is the steady state nucleation rate and τ the incubation time. Using this equation the measured crystal size distribution was compared with calculated distributions, taking the observed nucleation and growth rates deduced for 450° C, Figs 2 and 4, and using various values for τ. The final distributions obtained depend on the ratio of $I(t)/I_{ss}$ over the entire annealing period [33], and two calculated distributions are shown in Figs 7b and c. The distribution deduced using an incubation time of 8 min is in better agreement with the experimental results, and an even better agreement should, in principle, be obtained using a longer incubation time. The nucleation curve of Fig. 4 confirms, however, that the incubation time cannot be longer than about 5 min. Thus, it is concluded that the general form of the crystal-size distribution is consistent with the nucleation data, but that it is difficult, despite the large number of crystals counted, to use the distribution to deduce details of the nucleation process.

5. Conclusions

In the present study, ribbon samples of Ni–Si–B alloy have been prepared under conditions of careful control. The helium atmosphere used for melt-spinning, as well as the choice of a rapid cooling rate, have resulted in a material relatively resistant to crystallization with a very slow bulk nucleation rate. The slow bulk nucleation rate is a direct consequence of avoiding internal heterogeneous nucleation, and as a corrollary the material exhibits sensitivity to surface crystallization.

The surface crystallization has been shown to be a consequence of abundant nucleation in the surface layer following selective oxidation of the silicon. It appears most likely that nucleation is enhanced because the remaining glass has a less-stable composition. A technical consequence of this is the possibility to obtain more massive samples by direct casting, provided surface contamination, and enhanced crystallization, can be avoided.

The nucleation observed in the glass volume appears fully consistent with a homogeneous nucleation mechanism at high temperature and nucleation on quenched-in heterogeneities at low temperatures. These quenched-in heterogeneities appear more likely to be short-range ordered clusters of the alloying

elements rather than associated with impurity atoms. Further experiments are planned, however, to examine this point.

Acknowledgements

We are grateful to Dr M. A. Morris for considerable assistance with the melt spinning of the present alloy, and to Dr Matthieu of the Department of Materials, Technical High School of Lausanne, for performing the Auger analysis. We also thank the Swiss National Science Foundation for partial support of one of us (Marc-Henri Zuercher).

References

1. U. KOSTER and U. HEROLD, "Topics in Applied Physics", Vol. 46, edited by H. J. Guntherodt and H. Beck (Springer-Verlag, Berlin, 1981) p. 225.
2. J. W. CHRISTIAN, "The Theory of Transformations in Metals and Alloys" (Pergamon, Oxford, 1975).
3. H. A. DAVIES, *Phys. Chem. Glasses* **17** (1976) 159.
4. D. G. MORRIS, *Acta Metall.* **31** (1983) 1479.
5. R. S. TIWARI, S. RANGANATHAN and M. VON HEIMENDAHL, *Z. Metallkde* **72** (1981) 563.
6. D. G. MORRIS, *Acta Metall.* **29** (1981) 1213.
7. K. MULLER and M. VON HEIMENDAHL, *J. Mater. Sci.* **17** (1982) 2525.
8. U. KOSTER and H. BLANKE, *Scripta Metall.* **17** (1983) 495.
9. A. J. DREHMAN and A. L. GREER, *Acta Metall.* **32** (1984) 323.
10. G. K. DEY and S. BANERJEE, *Mater. Sci. Engng* **73** (1985) 187.
11. A. L. GREER, *Acta Metall.* **30** (1982) 171.
12. I. W. DONALD and H. A. DAVIES, *J. Mater. Sci.* **15** (1980) 2754.
13. A. INOUE, T. MASUMOTO, M. KIKUCHI and T. MINEMURA, *J. Jpn Inst. Metals* **42** (1978) 294.
14. *Idem, Sci-Rep. R.I.T.U.* **A27** (1979) 127.
15. M. HAGIWARA, A. INOUE and T. MASUMOTO, *Met. Trans.* **12A** (1981) 1027.
16. D. G. MORRIS, *Acta Metall.* **32** (1984) 837.
17. O. PILZ and P. L. RYDER, in "Rapidly Quenched Metals", edited by S. Steeb and H. Warlimont (North-Holland, Amsterdam, 1985) p. 377.
18. D. PAVUNA, *J. Mater. Sci.* **16** (1981) 2419.
19. E. E. UNDERWOOD, in "Quantitative Microscopy", edited by R. T. DeHoff and Rhines (McGraw-Hill, New York, 1968) Ch. 6.
20. R. T. DeHOFF, "Quantitative Metallography, Techniques for Metals Research", Vol. II, edited by R. F. Bunshah (Interscience, New York, 1968) p. 221.
21. U. KOSTER and U. HEROLD, Proceedings 4th International Conference on Rapidly Quenched Metals, Sendai, Japan Institute of Metal, edited by T. Masumoto and K. Suzuki (Japan Institute of Metals, Sendai, 1981) 717.
22. K. MULLER and M. VON HEIMENDAHL, *J. Mater. Sci.* **17** (1982) 2525.
23. F. A. PONCE and S. HAHN, *Mater. Res. Soc. Symp. Proc.* **31** (1984) 153.
24. U. KOSTER, in "Phase Transformations in Crystalline and Amorphous Alloys", edited by B. L. Mordike (Deutsche Gesellschaft fur Metallkunde, Oberursel, 1983) p. 113.
25. M. VON HEIMENDAHL and G. KUGLSTATTER, *J. Mater. Sci.* **16** (1981) 2405.
26. B. CANTOR and R. W. CAHN, in "Amorphous Metallic Alloys", edited by F. E. Luborsky (Butterworth, London, 1983).
27. C. V. THOMPSON and F. SPAEPEN, *Acta Metall.* **27** (1979) 1856.
28. K. F. KELTON, A. L. GREER and C. V. THOMPSON, *J. Chem. Phys.* **79** (12) (1983) 6261.
29. I. GUTZOW, *Contemp. Phys.* **21** (1980) 121.
30. C. V. THOMPSON, A. L. GREER and F. SPAEPEN, *Acta Metall.* **31** (1983) 1883.
31. H. BLANKE and U. KOSTER, "Rapidly Quenched Metals", edited by S. Steeb and H. Warlimont (North-Holland, Amsterdam, 1985) p. 227.
32. D. KASHCHIEV, *Surf. Sci.* **14** (1969) 209.
33. I. GUTZOW, D. KASHCHIEV and I. AVRAMOV, *J. Non-Cryst. Solids* **73** (1985) 477.

Received 20 February
and accepted 29 April 1987